# Influence of annealing temperature on the performance of Ge film and photon-counting imaging system

**Feifei Zhao (赵菲菲)[1,2*], Baosheng Zhao (赵宝升)[1], Xiaofeng Sai (赛小锋)[1], Xinghua Zhang (张兴华)[1,2], Yonglin Wei (韦永林)[1], and Wei Zou (邹 玮)[1]**

[1]*State Key Laboratory of Transient Optics and Photonics, Xi'an Institute of Optics and Precision Mechanics, Chinese Academy of Sciences, Xi'an 710119, China*

[2]*Graduate University of Chinese Academy of Sciences, Beijing 100049, China*

**E-mail: free.ff@163.com*

Received July 22, 2009

Compared with the traditional image intensifier with phosphor screen readout, the photon-counting imaging detector with charge induction readout is more beneficial in several aspects (e.g., good imaging properties and time resolution) to astronomy, reconnaissance, bioluminescence, and materials research. However, the annealing temperature during the tube-making process can affect the properties of the Ge film, and consequently impair the performance of the detector. Therefore, the influence of annealing temperature on Ge film and on the detector is studied in order to determine the crucial parameters. The Ge films are prepared on ceramic and quartz glass by the use of an electron gun. They are analyzed by scanning electron microscope (SEM), high-resistance meter, and X-ray diffraction (XRD). The results show that the optimum substrate and annealing temperature are ceramic plate and 250 °C, respectively.

*OCIS codes:* 160.6000, 030.5260, 110.2970, 100.0100.
*doi: 10.3788/COL20100804.0361.*

The world space observatory-ultraviolet (WSO-UV) is a space telescope project led by Russia, with contributions from several other countries. The mission involving a long-slit spectrograph instrument provides low-resolution spectra in the range of 102–320 nm in China. Therefore, the study on two photon-counting detectors in the ranges of 102–170 and 160–320 nm is carried out.

The photon-counting imaging detector, which is characterized by both high time resolution and good imaging properties, is superior to the traditional image intensifier with phosphor screen readout[1] as well as to hybrid sensors, such as intensified charge-coupled devices (ICCDs)[2] and electron-multiplying charge-coupled devices (EMCCDs)[3,4] in the field of imaging at very low flux level and in the solar-blind ultraviolet (UV) range. Compared with the sealed imaging detector tubes with position-sensitive anode[5−7], the photon-counting detector[8−10] with charge induction readout is beneficial in several aspects, such as the abilities to avoid image distortion produced by secondary electron, eliminate noise due to quantized charge collection, simplify the electronic design requirements, and so on. However, the annealing temperature during the encapsulation process and photocathode preparation may affect the properties of the Ge film, and consequently impair the performance of the detector (e.g., the position resolution). Therefore, the objectives of this study are to research the influence of annealing temperature on Ge film and on the detector and to determine the crucial parameters.

Figure 1 shows the schematic cross-section of a near-UV (NUV) sealed tube imaging detector. The components of the detector are sealed in a vacuum tube, which is required for their operation. A semitransparent cesium telluride photocathode is deposited on the input window to accommodate the wavelength range of 160–320 nm. During the technological process, these tube parts are annealed in a vacuum chamber for 40 h prior to the preparation of the photocathode. The entire process of preparing a sealed tube creates many problems, one of which is the influence of annealing temperature on the Ge films. To simplify the experiment, a photon-counting imaging system is used, whose configuration and operating flow are shown in Fig. 2.

This system utilizes a chevron stack of microchannel plates (MCPs), each with a length-to-diameter ratio

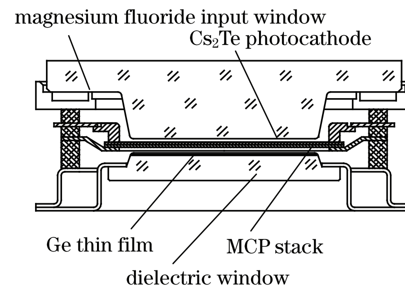


Fig. 1. Schematic cross-section of NUV sealed tube. MCP: microchannel plate.

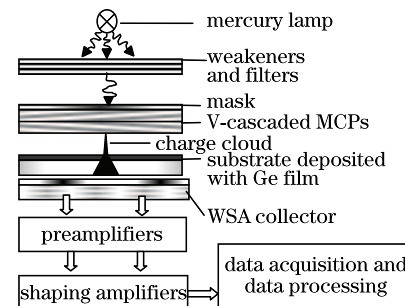


Fig. 2. Sketch of experimental photon-counting imaging system. WSA: wedge and strip anode.

 © 2010 Chinese Optics Letters

of 40:1. When the charge induction readout is adopted, various position-sensitive anodes can be attached from outside the sealed tube. The wedge and strip anode (WSA)[11−14] is applied due to its relatively simple configuration and high resolution. The single photon stream can be obtained via atmospheric dispersion, some weakeners, and narrow-band optical filters. A photo-electron emitted from the photocathode is accelerated toward the stack of MCPs and then multiplied, forming a charge cloud. This event charge is collected on the Ge film, which serves to localize the event while allowing discharge over a longer time period. The WSA detects the event charge by capacitive coupling from a few millimeters behind the Ge film. Any localized charge arriving at the Ge film is dispersed with the resistor-capacitor (RC) time constant determined by the Ge film resistance and the capacitance density determined by the spacing between the Ge film and the WSA anode[15]. The principle of the photon-counting imaging system shows that the resistance and structure of the Ge film can affect the performance of this imaging system.

The Ge films were grown on quartz glass and ceramic plate substrates by vacuum deposition with an e-type electron beam. Prior to this, the ceramic plate was immersed in $NH_4OH/H_2O_2/H_2O$ and 0.5% HCl solutions in sequence to wipe off the grains and metal contamination. After washing with distilled water and drying, the ceramic plate was placed into a vacuum furnace and annealed at 700 °C for 4 h to eliminate impurities. Organic solvents were used to clean the quartz glass. The Ge films were deposited on substrates under a residual pressure of $9 \times 10^{-4}$ Pa at room temperature (20 °C). The Ge deposition rate was maintained constant at 1 nm/s. Figure 3 shows the photographs of two kinds of substrates on which Ge films are deposited. To study the thermal effect, annealing was performed at 150, 250, 350, 450, and 550 °C for 8 h under a residual pressure of $3 \times 10^{-4}$ Pa. In this letter, quartz glass and 99% ceramic plates are chosen as substrates because of their excellent properties. For instance, the glass phase of 99% ceramics is small and its polycrystalline structure is perfect. Therefore, the very low dielectric loss of ceramics is only induced by the conductance process. So is quartz glass due to its compact structure. The crystallinity of the Ge films was examined by X-ray diffraction (XRD). A scanning electron microscope (SEM) was used to examine the microstructure of the films.

After annealing, the sheet resistance of Ge thin films was measured using a high-resistance meter. Table 1 shows that as the annealing temperature increases from 150 to 350 °C, the sheet resistance increases gradually due to the different expansion coefficients of the Ge films and substrates. The resistance starts to decrease when the temperature is above 350 °C, which can be attributed to the microstructure variation. However, this trend becomes smoother as the temperature goes up to more than 450 °C. In addition, there is a difference in the effect of the annealing process on the two substrates. The sheet resistance of Ge films deposited on ceramic plates changes, but not as sharply as that of films deposited on the quartz glass, which indicates the better thermal stability of Ge films on ceramics.

**Table 1. Sheet Resistance of Ge Thin Films on Different Substrates at Different Annealing Temperatures**

| No. | Temperature (°C) | Sheet Resistance (Ω/□) | |
|---|---|---|---|
| | | Quartz Glass | Ceramic Plate |
| 1 | 20 | $1.6\times10^7$ | $4.0\times10^7$ |
| 2 | 150 | $1.5\times10^8$ | $4.8\times10^7$ |
| 3 | 250 | $5.6\times10^8$ | $1.2\times10^8$ |
| 4 | 350 | $5.4\times10^8$ | $3.8\times10^8$ |
| 5 | 450 | $1.5\times10^5$ | $3.1\times10^4$ |
| 6 | 550 | $1.8\times10^3$ | $1.1\times10^4$ |

Figure 4 shows the XRD patterns of Ge films deposited on two different substrates at different annealing temperatures. Before annealing, the Ge films on both substrates have a cubic amorphous structure, because there are only three wide, weak peaks corresponding to Ge (111), Ge (220), and Ge (311), while the wide peak at $2\theta = 20°$ (Fig. 4(a)) and the sharp peaks (Fig. 4(b)) are the diffraction peaks of the quartz glass and the ceramics, respectively. Figure 4(a) shows that the structure of the film on the quartz glass becomes crystalline at 550 °C. The structure of the Ge film on ceramics starts to change from amorphous to crystalline at 450 °C (Fig. 4(b)). The crystalline increases with increasing

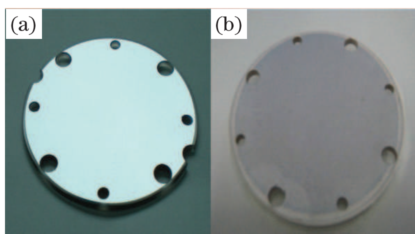

Fig. 3. Photographs of Ge films deposited on (a) quartz glass and (b) ceramic plate.

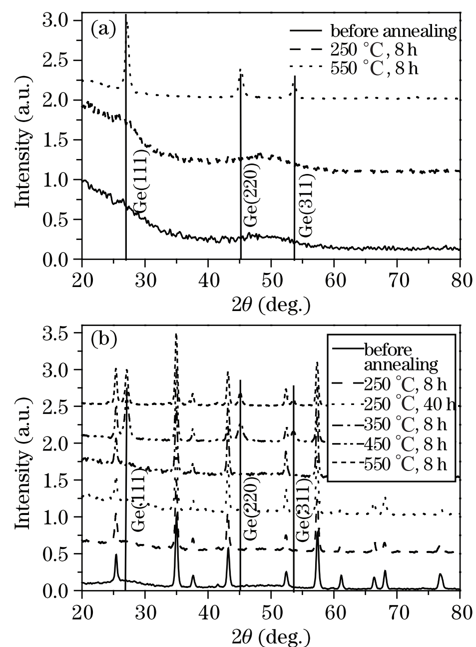

Fig. 4. XRD patterns of Ge films deposited on different substrates at different annealing temperatures. (a) Quartz glass and (b) ceramic plate.

the annealing temperature; the full-width at half-maximum (FWHM) drops from 62.1% at 450 °C to 44.6% at 550 °C (Fig. 4(b)). Figure 4(b) also shows that there is no difference between the structures of the Ge films annealed at 250 °C for 8 h and for 40 h.

The effects of varying annealing temperature on the surface morphology of Ge films were also investigated. The crystallinity of the Ge films deposited on both the quartz glass and ceramic plate is amorphous (Fig. 5). The films deposited on the quartz glass are even more amorphous, which is attributed to the different surface smoothnesses. Moreover, the films pile up on the crystal boundary of the ceramic plate. This phenomenon results in higher resistance of films deposited on ceramic plate under the same parameters. Figure 5 shows that the annealing temperature has a marked effect on the thin films, which is consistent with the results of the XRD experiment. When the annealing temperature does not exceed 350 °C, the morphology changes slightly and the crystallinity remains amorphous before annealing. The crystal grains occur until 450 °C, and grow when the temperature increases. Figure 5(e) does not show any crystal grains, because the grains are too small and the film is very compact. The grains can be easily seen using a transmission electron microscope.

In the earlier experiments, the results indicate that both the resistance and thickness of the Ge film have dramatic effects on the properties of the system, which is relatively high when the resistance is below 300 MΩ/□ with an optimum thickness of 100 nm. From the above analysis, we can conclude that the thermal stability of films on ceramic plate is superior. The resistance is still in this range after annealing at 250 °C, with little change to the microstructure. Although the influence is less when the temperature is below 250 °C, the annealing time has to be prolonged so that the degree of the vacuum chamber does not reach $10^{-7}$ Pa during the preparation process of sealed tubes. We set the ceramic plate with Ge film after annealing at 250 °C for 40 h down in the imaging system, and then compared the results with the images taken before annealing. In addition, we also performed this experiment after annealing at 550 °C to determine the performance of the imaging system when the resistance of the Ge film is reduced by several orders of magnitude (see Table 1). The self-designed resolution mask was used to examine the spatial resolution of this imaging system, and was set down on the front surface of the first MCP (see Fig. 2). The stack of MCPs was driven by a bias voltage of 1850 V. The distance between a MCP stack exit and the Ge film was 1 mm, and an additional 300 V was applied so that the electron avalanche produced a well-defined footprint on the Ge film. Figure 6 shows the mask and photon-counting images. The results show that there is little difference between the photon-counting images of the resolution mask before and after annealing at 250 °C except that the counting rate descends from 900 to 800 count/s. However, the position resolution of the image is so low that no slit can be distinguished when the Ge film is annealed after 550 °C. The reason is that the transmission of the signals to the WSA becomes lower with the consequent deterioration of the signal-to-noise ratio (SNR)[16].

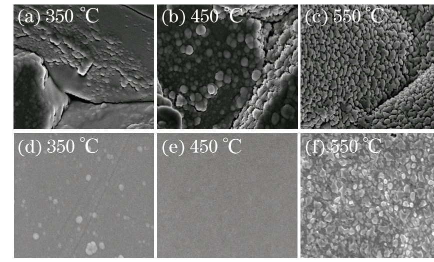


Fig. 5. SEM photographs of Ge thin films on different substrates at different annealing temperatures. (a), (b), (c) quartz glass, (d), (e), (f) ceramic plate.

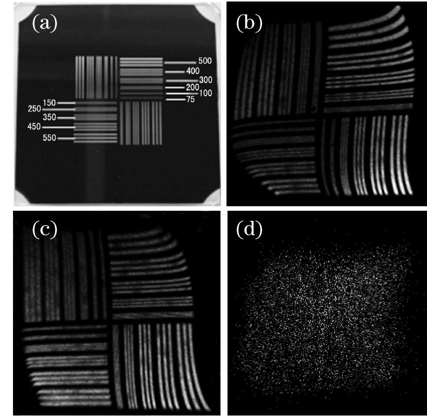


Fig. 6. Mask and photon counting images with Ge films on ceramic substrate. (a) Mask, (b) before annealing, (c) after annealing at 250 °C, and (d) after annealing at 550 °C.

In conclusion, the influence of annealing temperature on the characteristics of Ge films on quartz glass and ceramic plate is investigated. The results show that as the annealing temperature increases from 150 to 350 °C, the sheet resistance of the Ge film also gradually increases due to the different expansion coefficients of the Ge film and the substrates. The resistance is reduced by several orders of magnitude when the temperature is above 350 °C, which can be attributed to the microstructure variation from amorphous to crystalline. Moreover, the thermal stability of Ge films on ceramic substrates is better than that on quartz glass substrates. The experiments on device performance indicate that low sheet resistance of Ge film with the same thickness can impair the position resolution of the photon-counting imaging system with charge induction readout. However, the effect of annealing at 250 °C on the resolution of the system is slight; therefore, annealing at 250 °C and ceramic substrates adopted in the manufacture process are the best choice.

This work was supported by the National Natural Science Foundation of China under Grant No. 10878005.

## References

1. W. Li, B. Zhao, F. Zhao, and X. Cao, Acta Photon. Sin. (in Chinese) **38,** 1353 (2009).
2. M. Lindner, S. Elstein, and P. Lindner, Proc. SPIE **3434,** 22 (1998).

3. X. Xu and J. Guo, Proc. SPIE **4919,** 536 (2002).
4. K. Hoepfner and W. Schmidt-Parzefall, Nucl. Instr. and Meth. in Phys. Res. A **440,** 46 (2000).
5. X. Zhang, B. Zhao, Z. Miao, X. Zhu, Y. Liu, and W. Zou, Acta Phys. Sin. (in Chinese) **57,** 4238 (2008).
6. J. H. Barnes IV and G. M. Hieftje, Int. J. Mass Spectrom. **238,** 33 (2004).
7. O. Jagutzki, V. Mergel, K. Ullmann-Pfleger, L. Spielberger, U. Meyer, R. Dörner, and H. Schmidt-Böcking, Proc. SPIE **3438,** 322 (1998).
8. O. Jagutzki, J. S. Lapington, L. B. C. Worth, U. Spillman, V. Mergel, and H. Schmidt-Böcking, Nucl. Instr. and Meth. in Phys. Res. A **477,** 256 (2002).
9. J. S. Lapington, S. Chakrabati, T. Cook, J. C. Gsell, and V. T. Gsell, Nucl. Instr. and Meth. in Phys. Res. A **513,** 159 (2003).
10. J. M. Maia, D. Mörmann, A. Breskin, R. Chechik, J. F. C. A. Veloso, and J. M. F. dos Santos, Nucl. Instr. and Meth. in Phys. Res. A **580,** 373 (2007).
11. X. Zhu, B. Zhao, Y. Liu, Z. Miao, X. Zhang, and W. Zou, Acta Opt. Sin. (in Chinese) **28,** 1925 (2008).
12. X. Zhang, B. Zhao, Z. Miao, W. Li, X. Zhu, Y. Liu, and W. Zou, Chin. Opt. Lett. **6,** 661 (2008).
13. C. Martin, P. Jelinsky, M. Lampton, R. F. Malina, and H. O. Anger, Rev. Sci. Instrum. **52,** 1067 (1981).
14. O. H. W. Siegmund, M. Lampton, J. Bixler, S. Bowyer, and R. F. Malina, IEEE Trans. Nucl. Sci. **33,** 724 (1986).
15. M. S. Dixit, J. Dubeau, J. P. Martin, and K. Sachs, Nucl. Instr. and Meth. in Phys. Res. A **518,** 721 (2004).
16. G. Battistoni, P. Campana, V. Chiarella, U. Denni, E. Iarocci, and G. Nicoletti, Nucl. Instrum. Meth. Phys. Res. A **202,** 459 (1982).